Low-bandgap nonfullerene acceptor based on thieno[3,2-b]indole core for highly efficient binary and ternary organic solar cells

Chemical Engineering Journal 427 (2022) 131674

Contents lists available at ScienceDirect

Chemical Engineering Journal

journal homepage: www.elsevier.com/locate/cej

Low-bandgap nonfullerene acceptor based on thieno[3,2-*b*]indole core for highly efficient binary and ternary organic solar cells

Liang Xie [a,1], Yang Zhang [b,1], Wenliu Zhuang [c,d,1], Sang Young Jeong [e], Qingzhen Bian [f], Huangfen Li [a], Jiamin Cao [a,*], Wanqing Liu [a], Hua Tan [g,*], Han Young Woo [e], Jian Zhang [b,*], Ergang Wang [d,h,*]

[a] *Key Laboratory of Theoretical Organic Chemistry and Functional Molecule of Ministry of Education, Hunan Provincial Key Laboratory of Controllable Preparation and Functional Application of Fine Polymers, School of Chemistry and Chemical Engineering, Hunan University of Science and Technology, Xiangtan 411201, China*
[b] *School of Materials Science and Engineering, Engineering Research Center of Electronic Information Materials and Devices, Ministry of Education, Guangxi Key Laboratory of Information Materials, Guilin University of Electronic Technology, 1st Jinji Road, Guilin 541004, China*
[c] *Advanced Research Center for Polymer Processing Engineering of Guangdong Province, Guangdong Industry Polytechnic, Guangzhou 510300, China*
[d] *Department of Chemistry and Chemical Engineering/Applied Chemistry, Chalmers University of Technology, Göteborg SE-41296, Sweden*
[e] *Department of Chemistry, KU-KIST Graduate School of Converging Science and Technology, Korea University, Anam-ro 145, Seoul 02841, Republic of Korea*
[f] *Biomolecular and Organic Electronics, Department of Physics, Chemistry and Biology (IFM), Linköping University, Linköping 58183, Sweden*
[g] *School of Materials Science and Engineering, Jiangsu Collaboration Innovation Center of Photovoltaic Science and Engineering, Jiangsu Engineering Laboratory of Light-Electricity-Heat Energy-Converting Materials and Applications, National Experimental Demonstration Center for Materials Science and Engineering, Changzhou University, Changzhou 213164, China*
[h] *School of Materials Science and Engineering, Zhengzhou University, Zhengzhou 450001, China*

ARTICLE INFO

Keywords:
Frontier energy levels
Nonfullerene acceptors
Organic solar cells
Power conversion efficiency
Thieno[3,2-b]indole

ABSTRACT

A low-bandgap nonfullerene acceptor (NFA) TIT-2FIC based on thieno[3,2-*b*]indole-thiophenes core has been developed. Compared with the analogue NFAs DTC(4Ph)-4FIC and IT-4F, TIT-2FIC exhibited remarkably red-shifted absorption, and up-shifted HOMO energy level. In addition, TIT-2FIC showed interesting universal miscibility with the donors nonfluorinated PBDB-T and fluorinated PM6, therefore the corresponding organic solar cells achieved promising power conversion efficiencies (PCEs) of 11.80% and 13.00%, respectively, which are higher compared to the counterpart IT-4F based cells. Furthermore, the ternary PM6:TIT-2FIC:Y6 cell pronounced a high PCE of 17.22%, being significantly improved from that of 16.04% for the binary PM6:Y6 cell. Similar improvement in PCEs from 13.41% to 14.46% was also observed in the ternary PM6:TIT-2FIC:IT-4F cell with TIT-2FIC as the third component. These results indicated that TIT-2FIC is universally applicable as an acceptor with nonfluorinated or fluorinated polymer donor materials in both binary and ternary cells.

1. Introduction

In the last few years, the great success in the development of nonfullerene acceptors (NFAs) has revived organic solar cells (OSCs), and the highest power conversion efficiency (PCE) of OSCs has soared up to over 18% [1-7]. This great breakthrough is based on the unique advantages of NFAs, such as low cost, broad and strong light absorption, tunable and suitable energy levels, and morphological stability [7-13]. So far, the highly efficient nonfullerene OSCs always employ wide- or medium-bandgap donor materials and low-bandgap NFAs for the complementary optical absorption [14-18]. Therefore, the development of efficient low-bandgap NFAs have attracted extensive attention.

As one of the three most important parameters for OSC devices, open-circuit voltage (V_{OC}) is roughly proportional to the difference between the highest occupied molecular orbitals (HOMO) of the donor materials and the lowest unoccupied molecular orbitals (LUMO) of the acceptor materials [19]. Therefore, high LUMO energy levels of NFAs should be maintained for achieving high V_{OC}. On the other hand, broad absorption of the active layers is prerequisites for high short-circuit current (J_{SC}), and thus raising of HOMO energy levels is an excellent strategy to reduce the optical bandgaps of NFAs and extend their absorption spectra. Further, studies have shown that HOMO energy levels

* Corresponding authors.
E-mail addresses: minjiacao@163.com (J. Cao), tanhua815@126.com (H. Tan), jianzhang@guet.edu.cn (J. Zhang), ergang@chalmers.se (E. Wang).
[1] These authors contribute equally to this work.

https://doi.org/10.1016/j.cej.2021.131674
Received 10 May 2021; Received in revised form 14 July 2021; Accepted 2 August 2021
Available online 9 August 2021

of donor–acceptor (D-A) molecules are mainly determined by the donor segments [19,20]. It was well known that enhancing the electron-donating ability of core unit can enhance intramolecular charge transfer (ICT) effect and reduce the optical bandgaps of NFAs [21-24]. In 2017, Jen *et al.* replaced the indacenodithieno[3,2-*b*]thiophene (IDTT) core of the innovative NFA ITIC with more electron-rich thiophene-thieno[3,2-*b*]thiophene-thiophene (4T), which endows the acceptor 4TIC with ~100 nm red-shifted absorption spectrum, much higher HOMO energy level, enhanced photocurrent, and consequently better photovoltaic performance in the resulting OSCs [22]. In 2018, Zhan *et al.* synthesized a fused-ring electron acceptor (IOIC3) based on naphtho [1,2-*b*:5,6-*b*′]dithiophene core with hexyloxy side-chains. Compared with hexyl substituted IOIC2, IOIC3 exhibits a narrower bandgap, red-shifted absorption spectra, and higher electron mobility. Thus the OSCs based on the PTB7-Th:IOIC3 show 40% higher PCE than the PTB7-Th:IOIC2-based devices (13.1% *vs* 9.33%) [23]. Recently, Ding *et al.* developed a series of A-D-A NFAs based on pentacyclic, hexacyclic, heptacyclic, and octacyclic CO-bridged units. Due to the stronger electron-donating capability and enhanced backbone planarity of donor units, these NFAs exhibited broader absorption, stronger light-harvesting capability, higher HOMO energy levels, and much higher photovoltaic performance compared to the IDT-based counterparts [25-29].

Carbazole and dithieno[3,2-*b*:2′,3′-*d*]pyrrole (DTP) are the excellent donor units for OSCs [30-32]. Since the advent of NFAs, carbazole was used as the center-group of donor core for NFAs [33-39]. Hsu *et al.* synthesized dithienocyclopentacarbazole (DTC)-based NFA DTC(4Ph)-4FIC. When it blended with J71, PBDB-T, or PM6 (also called PBDB-T-2F), over 10% PCE were achieved for the corresponding OSCs [33]. DTP was also employed as the end-group of donor core for NFAs by Tang *et al.*, and decent photovoltaic performance have been achieved [40,41]. Thieno[3,2-*b*]indole (TI), containing fused benzene, thiophene and pyrrole, may be considered as a transitional structure between carbazole and DTP (Fig. 1). Thieno[3,2-*b*]indole exhibits strong electron-donating ability and coplanarity, and it could enhance ICT effect and raise the HOMO and LUMO energy levels. Therefore, thieno[3,2-*b*]indole has attracted much attention and been used widely as the donor unit for constructing D-A donor polymers in OSCs or dye-sensitized solar cells (DSSCs) [42-45]. However, NFAs based on thieno[3,2-*b*]indole core have not been reported yet.

In this work, using thieno[3,2-*b*]indole fused with two thiophenes (thieno[2″,3″:3′,4′]cyclopenta[1′,2′:4,5]thieno[3,2-*b*]thieno[2′,3′:3,4] cyclopenta[1,2-*f*]indole) as the core, and 2-(5,6-difluoro-3-oxo-2,3-dihydro-1*H*-inden-1-ylidene)malononitrile (2FIC) as the end-groups, a low-bandgap small-molecule acceptor TIT-2FIC with asymmetric configuration has been designed and synthesized successfully (Fig. 1 and Scheme S1). The optical and electronic properties, charge carrier transport, film morphology, miscibility, molecular orientation and photovoltaic properties were systematically investigated. Compared with NFAs DTC(4Ph)-4FIC and IT-4F, TIT-2FIC possessed red-shift absorption and narrower bandgap of 1.41 eV, and higher HOMO energy level, thus resulting in much higher PCEs of 11.80% and 13.00% when blended with PBDB-T and PM6, respectively. Compared to conventional binary devices, ternary OSCs using additional donor or acceptor as a third component often exhibit improved photovoltaic performance, due to the enhanced light harvesting, optimized morphology, or reduced energy loss (E_{loss}) [46-49]. As expected, TIT-2FIC could be used as a third component to endow ternary PM6:TIT-2FIC:Y6 cells and PM6:TIT-2FIC:IT-4F cells with significantly improved PCEs of 17.22% and 14.46%, respectively.

2. Results and discussion

2.1. Materials synthesis and characterization

The synthesis procedure for TIT-2FIC is depicted in Scheme S1, and experiment details could be found in the Supporting Information. The starting materials 6-bromo-4-hexyl-4*H*-thieno[3,2-*b*]indole (**1**) and 2,6-dibromo-4-hexyl-4*H*-thieno[3,2-*b*]indole (**2**) were synthesized according to the literature [42-44]. Organotin compound **3**, derived from

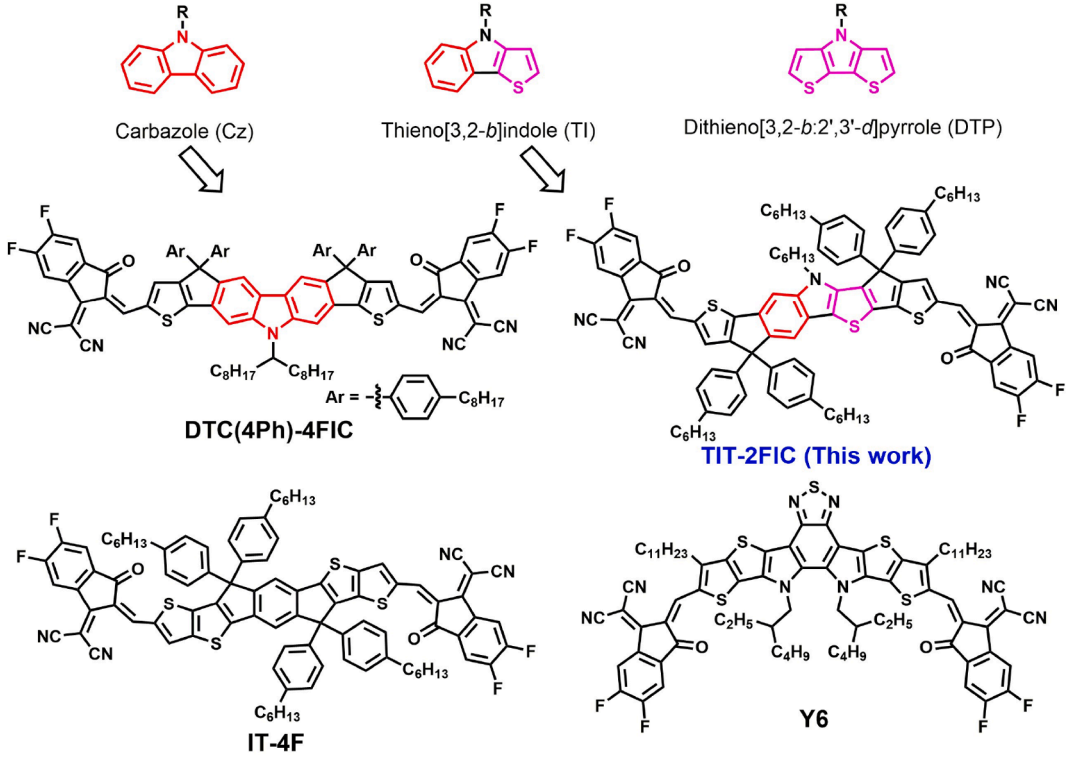

Fig. 1. The chemical structures of core segments Cz, TI, DTP and the related NFAs.

compound **2**, was reacted with ethyl 2-bromothiophene-3-carboxylate to obtain compound **4** through Stille coupling reaction. Then it was reacted with 4-hexylphenyl lithium to give the tertiary alcohol **5**, and key intermediate **6** was synthesized through Friedel-Crafts alkylation reaction. Vilsmeier-Haack reaction could convert compound **6** into dialdehyde compound **7**, and finally target NFA TIT-2FIC was obtained *via* Knoevenagel condensation with end-group 2FIC. TIT-2FIC and the intermediates were well-characterized by NMR spectra and mass spectra (Figure S1 & S2). TIT-2FIC can dissolve readily in common organic solvents such as dichloromethane, chlorobenzene, and chloroform. As measured by thermogravimetric analysis (TGA), TIT-2FIC shows excellent thermal stability with a high thermal decomposition temperature (T_d) of 322 °C (Figure S3).

2.2. Optical properties

The UV–vis-NIR absorption spectra of TIT-2FIC are shown in Fig. 2**a**, Figure S4a and the detailed data are summarized in Table S1. In dilute chloroform solutions (10^{-5} M), TIT-2FIC exhibited a strong main peak at 753 nm with extinction coefficient (ε) of 2.4×10^5 M^{-1} cm^{-1}, which is ca. 10% higher than those of carbazole analogue DTC(4Ph)-4FIC (2.2×10^5 M^{-1} cm^{-1}) [33] and benchmark NFA IT-4F (2.1×10^5 M^{-1} cm^{-1}) [50]. From solution to film, the peak is red-shifted to 806 nm with ~70 nm wider absorption range, indicating strong intermolecular interaction of TIT-2FIC in the solid state [51-53]. Calculated from the absorption edge (882 nm), the optical bandgap of TIT-2FIC film is 1.41 eV, which is much smaller than those of DTC(4Ph)-4FIC (1.61 eV) and IT-4F (1.53 eV). It is clear that TIT-2FIC exhibited complementary absorption spectrum with known polymers PBDB-T and PM6. More importantly, TIT-2FIC blend films possessed broader and more effective absorption than IT-4F blend films, especially in the range of 730–950 nm (Figure S4b), which is important to achieve high photocurrent for the resulting devices based on TIT-2FIC.

2.3. Electrochemical properties and theoretical calculations

As shown in Figure S5, cyclic voltammetry (CV) was employed to investigate the electrochemical properties of TIT-2FIC, and the electrochemical data are listed in Table S1. The oxidation onset potential (E_{ox}^{on}) of TIT-2FIC is 0.66 V, while the reduction onset potential (E_{red}^{on}) is −0.82 V. According to the empirical formula [54-57], the HOMO/LUMO energy levels of TIT-2FIC are estimated to be −5.46 eV and −3.98 eV, respectively. Compared with carbazole-based NFAs [33,37], TIT-2FIC possessed ~0.34–0.40 eV higher HOMO energy level and approximate LUMO energy level. The up-shifted HOMO energy level resulted from the stronger electron-donating ability of thieno[3,2-*b*]indole in contrast with carbazole, and this should be responsible for the narrower bandgap of TIT-2FIC. More importantly, the replacement of carbazole core with stronger electron-donating thieno[3,2-*b*]indole could only raise the HOMO energy level of the target NFAs without affecting the LUMO level and the V_{OC} of the resulting devices. It is noteworthy that HOMO offset between TIT-2FIC and PM6 is extremely small, which however should not be regarded as a hurdle for the photovoltaic performance since recent study has shown HOMO offset between donor and acceptor materials is not necessary for efficient OSCs [58]. In addition, TIT-2FIC possessed higher LUMO energy level and much higher HOMO energy level when compared with IT-4F, which leads to a narrower optical bandgap and is beneficial for higher V_{OC} and J_{SC} in the TIT-2FIC based devices.

Density functional theory (DFT) calculations at the ωB97XD/def2-SVP level were carried out to investigate optimal geometric configurations and molecular frontier orbitals for TIT-2FIC in comparison with DTC(4Ph)-4FIC and IT-4F (Fig. 2c and Figure S6). All these three NFAs have planar conjugated backbones with comparable conjugation path length in the central cores. However, it should be noted that different from centrosymmetric IT-4F and axisymmetric DTC(4Ph)-4FIC, TIT-2FIC is a totally asymmetric molecule. The energy levels calculated at the B3LYP-D3(BJ)/def2-SVP and ωB97XD/def2-SVP levels are both included in Table S1 for comparison, based on the optimized geometries

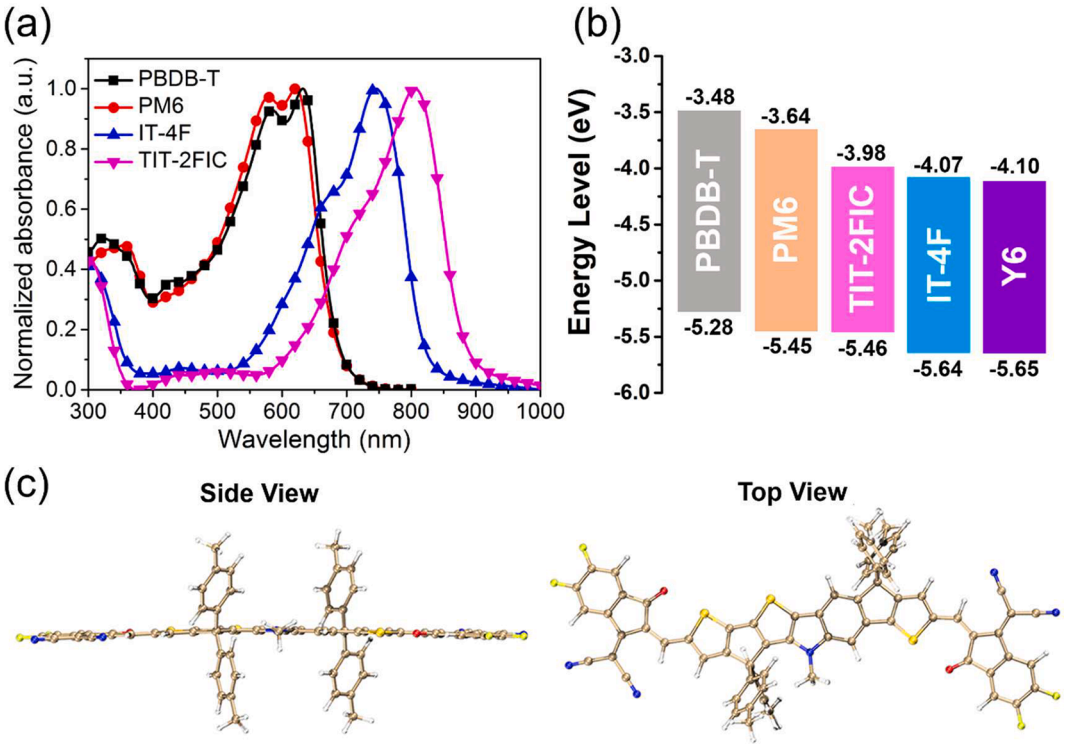

Fig. 2. a) UV–vis-NIR absorption spectra and b) energy diagram of PBDB-T, PM6, IT-4F, TIT-2FIC, and Y6. c) Optimized molecular geometries of TIT-2FIC (isovalue 0.02 a.u.).

at the corresponding level of theory. The calculated HOMO and LUMO levels at the B3LYP-D3(BJ)/def2-SVP level are −5.52 eV and −3.56 eV for TIT-2FIC, −5.70 eV and −3.54 eV for DTC(4Ph)-4FIC, and −5.66 eV and −3.61 eV for IT-4F, respectively, which are consistent well with the values deduced from the CV data. Compared to DTC(4Ph)-4FIC, TIT-2FIC exhibited much up-shifted HOMO energy levels for the narrower energy gaps, resulting from the replacement of carbazole core with thieno[3,2-*b*]indole. In addition, the calculated HOMO and LUMO levels at the ωB97XD/def2-SVP level also showed the same trends with the CV data (Table S1). For all the molecules, the HOMOs are mostly located on the electron-donating cores, while the LUMOs are slightly more localized on the electron-accepting units.

Time-dependent density functional theory (TD-DFT) calculations at the ωB97XD/def2-SVP level suggest the lowest excitations from the ground state (S_0) to the excited state (S_1) correspond to π-π* transitions with over 65% dominated by the HOMO → LUMO transitions for all the three molecules (Table S2). As shown in Table S3 and Figure S7, electron-hole analysis [59,60] of the transitions from the ground state to the excited states reveals that these NFAs feature high overlap of well distributed holes and electrons of the transitions, which may favor a higher oscillator strength of the corresponding transition, and the $S_0 \rightarrow S_1$ transitions have the highest oscillator strengths among all transitions of the same systems. The lowest excited-state vertical transition energies show a similar trend to the HOMO-LUMO gaps. As shown in Figure S8, we further simulated the UV–vis absorption of these NFA molecules in the gas phase under vacuum, and in solution with linear response polarizable continuum model (LR-PCM) [61] or state-specific polarizable continuum model (SS-PCM) models [62]. In these three models, the lowest excited-state vertical transition energies all followed the same trend: TIT-2FIC < IT-4F < DTC(4Ph)-4FIC, which are consistent with the optical data.

It can be found that DTC(4Ph)-4FIC belongs to C_{2v} symmetry and IT-4F belongs to C_{2h} symmetry, while TIT-2FIC belongs to C_1 symmetry. The variation in molecular symmetries can result in different molecular dipole moments. Intermolecular dipole interactions between conjugated molecules can drive neighboring molecules to form aggregates, particularly when the chromophore possesses a large dipole moment. To evaluate the molecular dipole moments of the studied structures more accurately, single point calculations at the level of PBE0/aug-cc-pVDZ were further performed based on the ωB97XD/def2-SVP optimized geometry. Calculated data show that compared to IT-4F with a molecular dipole moment of 0.000 D and DTC(4Ph)-4FIC with a molecular dipole moment of 0.417 D, the asymmetric TIT-2FIC has a much larger molecular dipole moment of 1.452 D, which is expected to favor charge transport through enhanced intermolecular interactions. It is also interesting to note that the frontier molecular orbitals (Figure S6) for these NFA molecules are strongly affected by the symmetries of the molecular structures, which are also observed in both the isosurface maps of electrostatic potential (ESP) on the van der Waals (vdW) surface and the isosurface maps of the vdW potential as shown in Figure S9. The ESP analysis shows that both TIT-2FIC and DTC(4Ph)-4FIC have a greater electronegativity difference over IT-4F and can form stronger electrostatic interaction to other molecules, enhancing their intermolecular interaction. For all the three NFAs, the isosurface map of the vdW potential evaluated by the Lennard-Jones 12–6 potential shows the regions (Figure S9, blue isosurface) where the dispersion attraction effect surpasses the exchange-repulsion effect are favorable physical adsorption zones for intermolecular packing and these regions are mainly facing to the plane of the conjugated backbones, beneficial to π-π stacking, and the most favorable adsorption sites are close to the core units of the NFA molecules, as a result of their backbone planarity and symmetry. Moreover, IRI-π analysis based on the recently proposed interaction region indicator (IRI) clearly indicates that these NFAs are ideal for π-π stacking, in consistence with the ESP and vdW analyses. From the above discussion of molecular dipole moments, electrostatic interaction, van der Waals interaction and IRI-π analyses, it is expected that the asymmetric TIT-2FIC can have enhanced intermolecular interaction, molecular packing and thus improved photovoltaic performance.

2.4. Photovoltaic performance of binary OSCs

To investigate the photovoltaic performance of NFA TIT-2FIC, binary OSCs with the device structure of ITO/PEDOT:PSS/active layer/PFN-Br/Al were firstly fabricated and the known polymer donor materials PBDB-T and PM6 were chosen. For comparison, the commercial NFA IT-4F with heptacyclic core was also used as acceptor for the fabrication of OSCs. After optimization, solar cells based on PBDB-T:TIT-2FIC achieved a decent PCE of 11.80%, with a V_{OC} of 0.805 V, a J_{SC} of 21.16 mA cm^{-2} and a fill factor (FF) of 69.34% (Fig. 3**a** and Table 1). Meanwhile, the control devices based on PBDB-T:IT-4F just exhibited a ~20% lower PCE of 9.56%, with a V_{OC} of 0.727 V, a J_{SC} of 19.07 mA cm^{-2} and a FF of 68.91%. Compared with the PBDB-T:IT-4F cell, a much higher V_{OC} of PBDB-T:TIT-2FIC cell may originate from the higher LUMO energy level of TIT-2FIC. Meanwhile, better absorption property of TIT-2FIC is beneficial for the much higher photocurrent of PBDB-T:TIT-2FIC cell. These trend also have been maintained for the cells using fluorinated PM6 as the donor. As a result, the PM6:TIT-2FIC device exhibited higher V_{OC} (0.905 *vs* 0.858 V) and J_{SC} (20.69 *vs* 19.95 mA cm^{-2}) when compared with the PM6:IT-4F device. Finally, a slightly lower FF of 69.42% in the case of PM6:TIT-2FIC led to comparable PCEs (13.00% *vs* 13.03%). The advantages of TIT-2FIC as acceptor was clearly observed as it can always show higher V_{OC} and J_{SC} in the resulting devices compared to the state-of-the-art acceptor IT-4F. Besides, it also exhibited much higher J_{SC} than its carbazole-based NFAs counterpart DTC(4Ph)-4FIC [33], due to the remarkable red-shift absorption.

The enhanced J_{SC} of TIT-2FIC based cells were confirmed by the external quantum efficiency (EQE) spectra as compared to the IT-4F based cells. As shown in Fig. 3b, solar cells based on PBDB-T:TIT-2FIC and PM6:TIT-2FIC both exhibited ~70 nm broader EQE spectra, thus higher calculated currents of 20.35 and 19.83 mA cm^{-2} were obtained. These boarder EQE response are consistent well with the absorption spectra of blend films (Figure S4b). In contrast, the calculated currents of PBDB-T:IT-4F and PM6:IT-4F cells are 18.66 and 19.64 mA cm^{-2}, respectively, which are in good agreement with the J_{SC} obtained from the *J-V* measurements. In addition, PBDB-T:TIT-2FIC cells showed slightly higher EQE response than PM6:TIT-2FIC cells in the range 560 nm to 840 nm due to the better absorption and higher photoluminescence (PL) quenching efficiency (Figure S4b and Figure S10).

To reveal the charge extraction and exciton dissociation properties, the photocurrent density (J_{ph}) versus the effective voltage (V_{eff}) measurements were conducted. As shown in Fig. 3c and Table S4, the exciton dissociation probabilities (P_{diss}), defined by $P_{diss} = J_{ph}^*/J_{sat}$ under the short-circuit current condition [41,63], are calculated to be 96.4% and 98.1% for PBDB-T:IT-4F and PBDB-T:TIT-2FIC cells, respectively. PBDB-T:TIT-2FIC cell also exhibited much higher charge collection probability (P_{coll}, defined by $J_{ph}^{\&}/J_{sat}$) of 90.7%. These values are consistent well with the higher FF for PBDB-T:TIT-2FIC cells, suggesting more efficient exciton dissociation compared to the PBDB-T:IT-4F cell [41,64]. On the other hand, the PM6:IT-4F cell possessed higher P_{diss} and P_{coll} for higher FF of 76.18% as compared to the PM6:TIT-2FIC cells. The light-intensity (P_{in}) dependence of J_{SC} was examined to investigate the bimolecular recombination behavior on current extraction. As shown in Fig. 3d, linear relationship is observed with α value (0.989, 0.999, 0.997, and 0.989) close to 1 for these four devices. Especially, PBDB-T:TIT-2FIC cells show the α value of 0.999, indicating negligible bimolecular recombination and more efficient current extraction [41]. The light-intensity dependent V_{OC} measurement indicated TIT-2FIC based devices possessed much less trap-assisted recombination than those of IT-4F based counterparts with smaller V_{OC} - P_{in} slope [41,65]. As a result, TIT-2FIC exhibited excellent photovoltaic performance with the minimal bimolecular and trap-assisted recombination when combining PBDB-T or PM6.

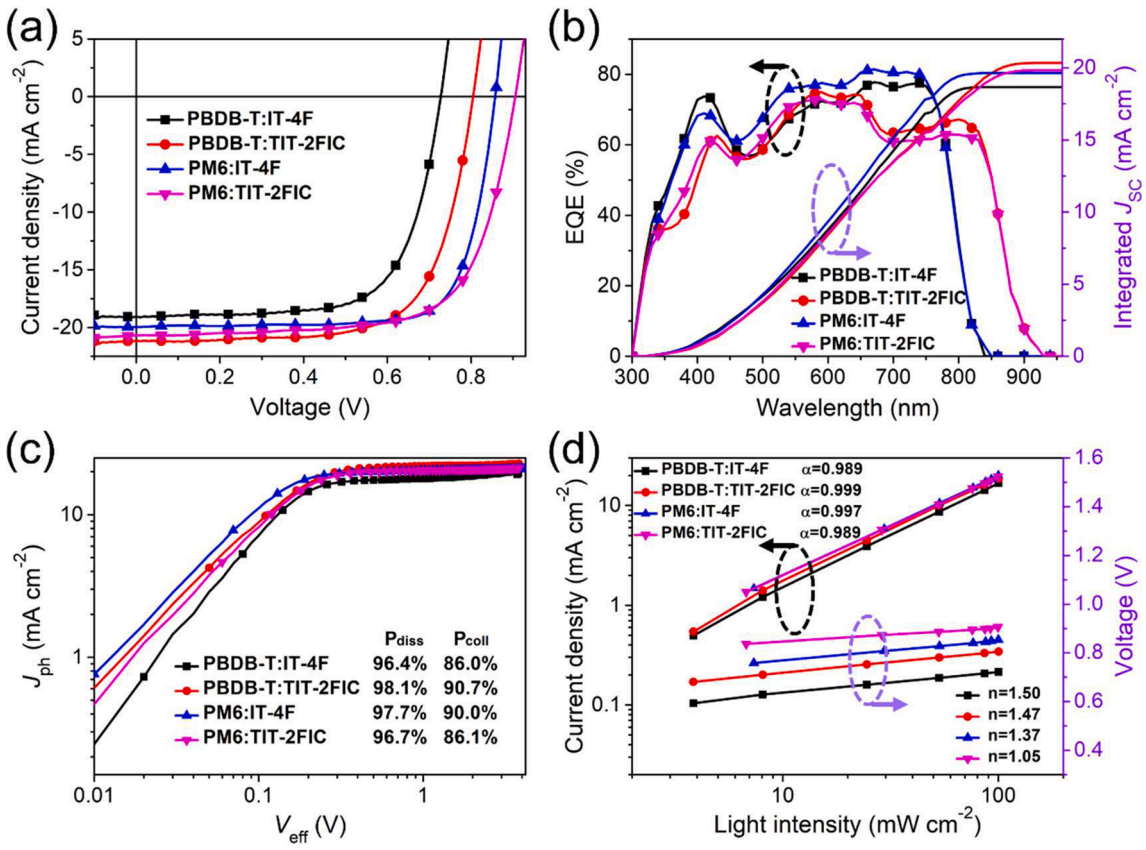

Fig. 3. a) *J-V* curves, b) EQE curves, c) J_{ph} *vs* V_{eff}, d) light intensity dependence of J_{SC} and V_{OC} of binary OSCs based on IT-4F or TIT-2FIC.

Table 1
Photovoltaic performance of the solar cells based on NFAs IT-4F or TIT-2FIC.

Active layer	V_{OC} [V]	J_{SC} [mA cm^{-2}]	FF [%]	PCE [%][a]	J_{EQE} [mA cm^{-2}]
PBDB-T:IT-4F	0.727	19.07	68.91	9.56 (9.48 ± 0.08)	18.66
PBDB-T:TIT-2FIC	0.805	21.16	69.34	11.80 (11.77 ± 0.03)	20.35
PM6:IT-4F	0.858	19.95	76.18	13.03 (12.87 ± 0.16)	19.64
PM6:TIT-2FIC	0.905	20.69	69.42	13.00 (12.80 ± 0.20)	19.83

[a] The average values are calculated from over 12 devices.

As measured by the space-charge limited current (SCLC), the electron and hole mobilities of PBDB-T:TIT-2FIC blend film are 3.83 × 10^{-4} and 2.65 × 10^{-4} cm^2 V^{-1} s^{-1}, respectively (Figure S11 and Table S5). These values are 50–70% higher than those of PBDB-T:IT-4F film. Similarly, PM6:TIT-2FIC blend film also exhibited higher charge carrier mobility than PM6:IT-4F film, probably originating from the larger molecular dipole moment and stronger intermolecular interactions of asymmetric NFAs [66]. Thus, higher photocurrents for the corresponding cells based on TIT-2FIC were achieved. The surface morphologies of the blend films were investigated by atomic force microscopy (AFM) as shown in Figure S12. PBDB-T:TIT-2FIC and PM6:TIT-2FIC blend films showed root-mean-square (RMS) roughnesses of 3.71 and 2.71 nm, respectively, while the roughness of PBDB-T:IT-4F and PM6:IT-4F blend films are 2.46 and 1.91 nm, respectively. These four blend films all exhibited uniform film morphology supporting their decent photovoltaic performance.

As discussed above, when combining with fluorinated PM6 or non-fluorinated PBDB-T, TIT-2FIC based OSCs achieved decent PCEs of 11.80% or 13.00%, indicating its universal compatibility. This point was proved by contact angle measurements and the Flory-Huggins model [67,68]. As shown in Figure S13 and Table S6, the surface free energy (γ_s) measured from the contact angles on water and diiodomethane (DIM) are 31.9, 34.1, 58.5, and 53.5 mN m^{-1} for PBDB-T, PM6, IT-4F, and TIT-2FIC, respectively. Further, the Flory-Huggins interaction parameters (χ) are calculated to be 3.59 for $\chi_{PBDB\text{-}T/IT\text{-}4F}$, 2.53 for $\chi_{PBDB\text{-}T/TIT\text{-}2FIC}$, 3.26 for $\chi_{PM6/IT\text{-}4F}$, and 2.16 for $\chi_{PM6/TIT\text{-}2FIC}$. It is clearly that TIT-2FIC shows the better miscibility with both PBDB-T and PM6 than IT-4F, according to AFM and charge carrier mobility results, and photovoltaics performance. Besides, $\chi_{PBDB\text{-}T/IT\text{-}4F}$ is the largest among the four pairs, which may be one of the main reasons for its low PCE of 9.56%.

2.5. Photovoltaic performance of ternary OSCs

The ternary OSCs with the device structure of ITO/PEDOT:PSS/PM6:TIT-2FIC:Y6/PDIN/Al were fabricated to further investigate the favorable role of TIT-2FIC in ternary devices as the third component. As shown in Fig. 4**a** and Table 2, various weight ratios of TIT-2FIC (0%, 5%, 10%, 15%, 100% by wt.) over the total acceptor weight were used to construct the ternary active layers and the total D/A weight ratio was kept as 1:1.2. For comparison, the control binary solar cells based on PM6:Y6 were fabricated and a decent PCE of 16.04% was achieved, consisting with the reported results [8]. After the addition of 5%~15% TIT-2FIC, all ternary OSCs based on PM6:TIT-2FIC:Y6 exhibited much better photovoltaic performance (16.69%~17.22%). Especially, the ternary OSCs with 10% TIT-2FIC achieved the highest PCE of 17.22%, with a V_{OC} of 0.870 V, a J_{SC} of 26.49 mA cm^{-2} and a FF of 74.73%. This significant improvement mainly originated from the enhanced photocurrent, which was confirmed by EQE spectra. As shown in Fig. 4b, the blend film containing 10% TIT-2FIC exhibited better EQE response than

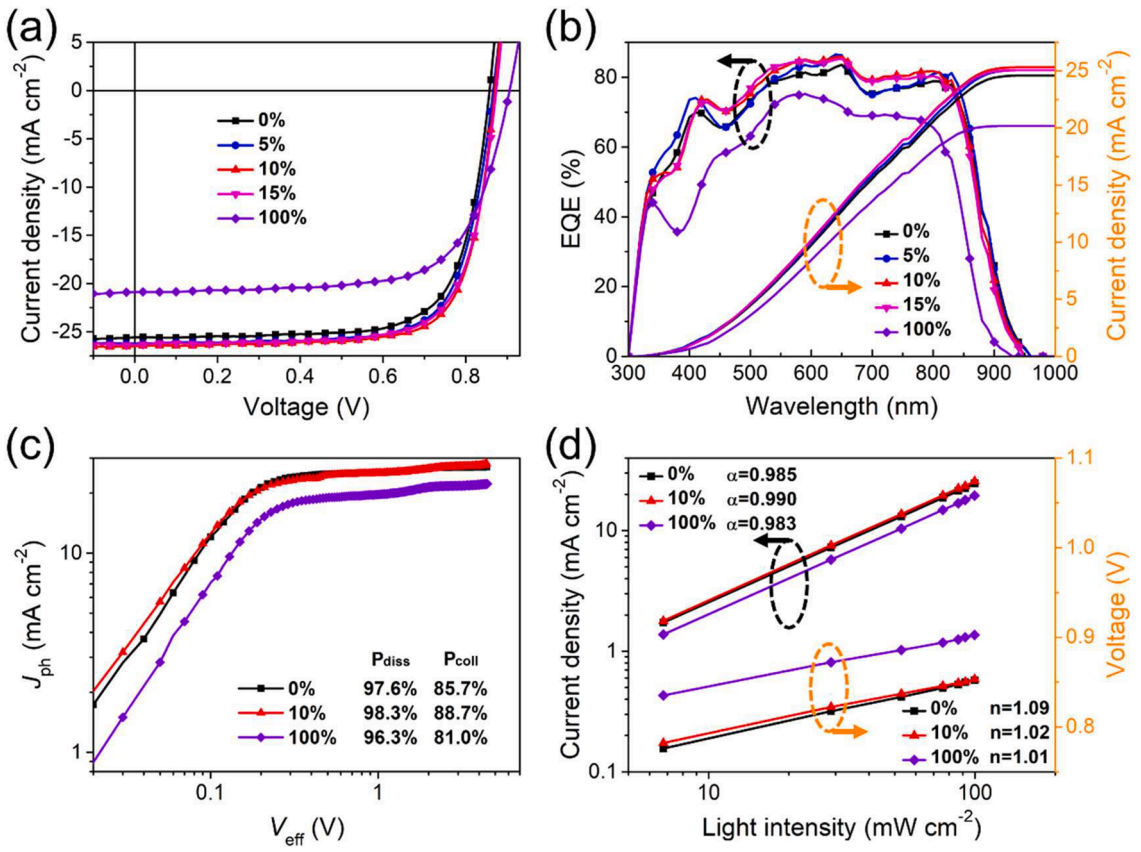

Fig. 4. a) *J-V* curves, b) EQE curves, c) J_{ph} *vs* V_{eff}, d) light intensity dependence of J_{SC} and V_{OC} of the PM6:Y6-based OSCs with different weight ratios of TIT-2FIC.

Table 2
Photovoltaic performance of the PM6:Y6-based solar cells with different weight ratios of TIT-2FIC.

TIT-2FIC in acceptors	V_{OC} [V]	J_{SC} [mA cm^{-2}]	FF [%]	PCE [%][a]	J_{EQE} [mA cm^{-2}]	E_{loss} [eV][b]
0%	0.857	25.58	73.16	16.04 (15.77 ± 0.27)	24.60	0.473
5%	0.866	26.24	73.44	16.69 (16.62 ± 0.07)	25.07	0.464
10%	0.870	26.49	74.73	17.22 (17.10 ± 0.12)	25.32	0.460
15%	0.873	26.35	73.46	16.90 (16.76 ± 0.24)	25.07	0.457
100%	0.905	20.87	69.03	13.05 (12.80 ± 0.25)	20.18	0.505

[a] The average values are calculated from over 12 devices.
[b] These values are calculated according to the formula $E_{loss} = E_g^{opt} - qV_{OC}$.

PM6:Y6 binary film almost in the whole absorption range, and the blend film possessed similar absorption spectra, especially for the enhanced absorption in the range of 660–820 nm (Figure S14). As a result, the calculated current from the EQE curve was improved to 25.32 mA cm^{-2} from 24.60 mA cm^{-2} of the PM6:Y6 binary cell. Meanwhile, the PM6:TIT-2FIC cells showed ~10% lower and ~35 nm narrower EQE response than other cells, leading to much lower photocurrent of 20.18 mA cm^{-2} and PCE of 13.05% eventually.

We also employed the photocurrent density (J_{ph}) versus the effective voltage (V_{eff}) measurements to investigate the charge extraction and exciton dissociation properties of ternary OSCs. As shown in Fig. 4c, the exciton dissociation probabilities (P_{diss}) are 97.6%, 98.3%, and 96.3% for PM6:Y6, PM6:10%TIT-2FIC:Y6 and PM6:TIT-2FIC cells, respectively. Then, P_{coll} of these three cells are 85.7%, 88.7%, and 81.0%, respectively. The higher P_{diss} and P_{coll} indicating efficient exciton dissociation are therefore beneficial for higher FF for the ternary OSCs with 10%TIT-2FIC. The light-intensity dependence of J_{SC} and V_{OC} measurement indicated that ternary OSCs with 10%TIT-2FIC exhibited negligible bimolecular and trap-assisted recombination, due to the α value of 0.990 and n value of 1.02 (Fig. 4d). These mean that ternary OSCs with 10%TIT-2FIC worked much better than the other two binary cells, which is in good agreement with its higher J_{SC} and FF obtained from the *J-V* measurements. As shown in Figure S15 in the Supporting Information, the ternary PM6:10%TIT-2FIC:Y6 films exhibited clear fibrillar structure and moderate RMS roughness of 1.03 nm when compared with the two binary films, which is beneficial to exciton dissociation and charge transport, and thus high FF in the optimized ternary OSCs [11,69].

For organic photovoltaics, the E_{loss} can be divided into three components: $E_{loss} = E_{gap} - qV_{OC} = (E_{gap} - qV_{OC}^{SQ}) + (qV_{OC}^{SQ} - qV_{OC}^{rad}) + (qV_{OC}^{rad} - qV_{OC})$. The qV_{OC}^{SQ} is the maximum voltage based on the Shockley-Queisser (SQ) limit, where it is assumed there is no absorption below the optical bandgap of the solar cell. The first term of ($E_{gap} - qV_{OC}^{SQ}$) is unavoidable and comes from the radiative recombination originating from the absorption above the bandgap. The second term of ($qV_{OC}^{SQ} - qV_{OC}^{rad}$) is an additional radiative recombination and comes from the absorption below the bandgap. The third term of ($qV_{OC}^{rad} - qV_{OC}$) comes from the nonradiative loss and the nonradiative channel has a clear contribution to the total voltage loss [70]. To explore the role of TIT-2FIC in the PM6:Y6 based ternary device, the nonradiative loss was further studied by EQE of electroluminescence (EL) (EQE_{EL}), which is the radiative quantum efficiency of solar cells when charges are

injected in the device. A reduced nonradiative loss results from an enhanced radiative quantum efficiency of solar cell (higher EQE_{EL} value). Although the pure TIT-2FIC demonstrates a high EQE_{EL}, comparable to Y6, the two binary PM6:Y6 and PM6:TIT-2FIC devices demonstrate almost the same EQE_{EL} (Fig. 5**a**). The nonradiative loss can be calculated by:

$$q\,\Delta V_{OC}^{\text{non-rad}} = -kT\ln(EQE_{EL})$$

Compared with the binary PM6:Y6 cell, the ternary device (with 10% TIT-2FIC) exhibited slightly larger non-radiative voltage loss of 0.28 V (*vs* 0.26 V for the binary cells), but the ternary cell possessed higher V_{OC} (0.870 *vs* 0.857 V) and lower E_{loss}. These results suggested that the enhancement of V_{OC} in the PM6:10%TIT-2FIC:Y6 cell came from the significantly reduced radiative loss and the loss from radiative channel was suppressed by the addition of the third component TIT-2FIC. Such conclusion could also be confirmed by the steady-state PL spectra (690 nm light excitation). As shown in Fig. 5b and Figure S16a, Y6:10%TIT-2FIC blend film exhibited ~35% higher PL emission intensity at 940 nm than that of Y6 film, and the emission peak of TIT-2FIC at 880 nm is apparently quenched in the blend film [69]. These results indicated there was efficient energy transfer process from TIT-2FIC to Y6, which was also supported by the overlap between absorption spectrum of Y6 and PL spectrum of TIT-2FIC (Fig. 5c). Additionally, acceptor-only devices were fabricated and Y6:10%TIT-2FIC device exhibited lower J_{SC} than that of Y6 based devices (Figure S16b), implying that no significant charge transfer occurs between TIT-2FIC and Y6 (Figure S16c) [63,69].

As shown in Fig. 5d-5f and Figure S17, grazing incidence wide-angle X-ray scattering (GIWAXS) was employed to investigate the molecular orientation of the ternary and binary blend films. These three blend films all exhibited obvious π-π stacking diffraction in the out-of-plane (OOP) direction with q value of ~1.7 $Å^{-1}$, indicating preferential face-on orientation. The PM6:Y6 and PM6:10%TIT-2FIC:Y6 blend films shown the same level of intensity response along the OOP direction, indicating that the addition of 10%TIT-2FIC does not interrupt the molecular stacking of PM6 and Y6, even though TIT-2FIC possesses significantly different chemical structure from Y6. In contrast, PM6:TIT-2FIC blend film exhibited significantly reduced (0 1 0) scattering peak in the OOP direction, showing weak molecular stacking, which partially explained the resulting relatively poor photovoltaic performance of 13.05%.

Furthermore, TIT-2FIC was used to improve the photovoltaic performance of PM6:IT-4F cells (Figure S18 and Table S7). After adding 30% or 50% TIT-2FIC, the PCEs of ternary were improved to 14.14% or 14.46% from 13.41% of the PM6:IT-4F binary cell, respectively. Similarly, the enhanced photocurrent of ~2 mA cm^{-2} mainly accounts for the improved photovoltaic performance.

3. Conclusion

In summary, using thieno[3,2-*b*]indole fused with two thiophenes as the core, and 2FIC as the end-groups, a NFA TIT-2FIC has been designed and successfully synthesized. Compared with NFA DTC(4Ph)-4FIC based on carbazole and IT-4F, TIT-2FIC exhibited over 80 nm red-shift absorption, low bandgap of 1.41 eV, and much suitable LUMO energy level. Using PBDB-T and PM6 as the donor materials, the corresponding binary OSCs exhibited decent PCEs of 11.80% and 13.00%, respectively. On the other hand, the PBDB-T:IT-4F and PM6:IT-4F cells showed PCEs of 9.56% and 13.03%, respectively. These binary OSCs results indicated that TIT-2FIC possess universal miscibility with both fluorinated and non-fluorinated polymer donors. Furthermore, 10%TIT-2FIC was added to the PM6:Y6 binary cells to construct ternary OSCs and the photovoltaic performance was improved to an impressive PCE of 17.22% from 16.04%, due to the better EQE response, more efficient charge extraction and exciton dissociation, and low voltage loss. Interestingly, it was found that the ternary OSCs based on PBDB-T:TIT-2FIC:IT-4F also achieved higher PCE than that of PBDB-T:IT-4F cells. Therefore, TIT-2FIC could be a commonly used additive for fabricating efficient ternary OSCs. Our results demonstrated that TIT-2FIC is a promising NFA with good compatibility with different donors and a robust third component for construction of ternary OSCs.

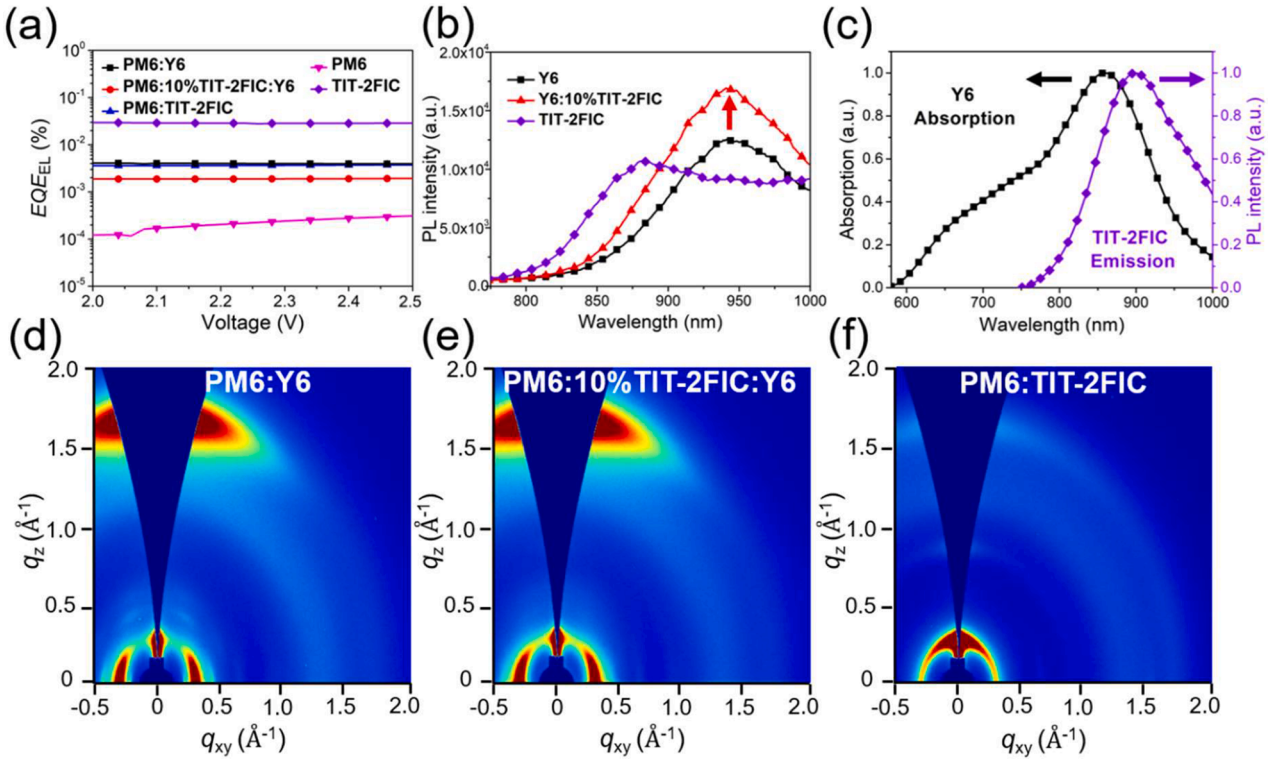

Fig. 5. a) EQE-EL curves. b) PL spectra of neat Y6, TIT-2FIC and Y6:10%TIT-2FIC films under 690 nm light excitation. c) The normalized absorption spectrum of Y6 and emission spectrum of TIT-2FIC. d,e,f) GIWAXS of the blend films.

Declaration of Competing Interest

The authors declare that they have no known competing financial interests or personal relationships that could have appeared to influence the work reported in this paper.

Acknowledgements

L.X., Y.Z. and W.Z. contributed equally to this work. J.C. acknowledges financial support from the National Natural Science Foundation of China (21604021), China Scholarship Council (CSC, 201808430041), Hunan Provincial Natural Science Foundation (2018JJ3141), School of Materials Science and Engineering, Jiangsu Engineering Laboratory of Light-Electricity-Heat Energy-Converting Materials and Applications (GDRGCS2020005). J. Z. acknowledges the support from the National Natural Science Foundation of China (61774050), Guangxi Natural Science Foundation Program (2019GXNSFGA245005), the Project (2020ZYZX2005), and the Bagui Scholars Program of Guangxi. E.W. thanks the Swedish Research Council (2016-06146, 2019-02345), the Swedish Research Council Formas, and the Wallenberg Foundation (2017.0186, 2016.0059) for financial support. W.Z. appreciates support from the China Scholarship Council (201908440047), NSFC project (11272093), Guangzhou Municipal Science and Technology Bureau (201804010501, 202002030362), Department of Education of Guangdong Province (2018GKTSCX041), and the Open Fund of the State Key Laboratory of Luminescent Materials and Devices (South China University of Technology, 2020-skllmd-07). H.Y.W. acknowledges the financial support from the National Research Foundation (NRF) of Korea (2019R1A6A1A11044070, 2020M3H4A3081814). H.T. acknowledges financial support from the Natural Science Foundation of the Jiangsu Higher Institutions of China (20KJA480004).

Appendix A. Supplementary data

Supplementary data to this article can be found online at https://doi.org/10.1016/j.cej.2021.131674.

References

[1] C. Yan, S. Barlow, Z. Wang, H. Yan, A.-K.-Y. Jen, S.R. Marder, X. Zhan, Nat. Rev. Mater. 3 (2018) 18003.
[2] P. Cheng, G. Li, X. Zhan, Y. Yang, Nat. Photonics 12 (2018) 131–142.
[3] J. Hou, O. Inganäs, R.H. Friend, F. Gao, Nat. Mater. 17 (2018) 119–128.
[4] Y. Cui, H. Yao, J. Zhang, K. Xian, T. Zhang, L. Hong, Y. Wang, Y. Xu, K. Ma, C. An, C. He, Z. Wei, F. Gao, J. Hou, Adv. Mater. 32 (2020) 1908205.
[5] Q. Liu, Y. Jiang, K. Jin, J. Qin, J. Xu, W. Li, J. Xiong, J. Liu, Z. Xiao, K. Sun, S. Yang, X. Zhang, L. Ding, Sci. Bull. 65 (2020) 272–275.
[6] Z. Wang, Z. Peng, Z. Xiao, D. Seyitliyev, K. Gundogdu, L. Ding, H. Ade, Adv. Mater. 32 (2020) 2005386.
[7] Y. Lin, J. Wang, Z.-G. Zhang, H. Bai, Y. Li, D. Zhu, X. Zhan, Adv. Mater. 27 (2015) 1170–1174.
[8] J. Yuan, Y. Zhang, L. Zhou, G. Zhang, H.-L. Yip, T.-K. Lau, X. Lu, C. Zhu, H. Peng, P. A. Johnson, M. Leclerc, Y. Cao, J. Ulanski, Y. Li, Y. Zou, Joule 3 (2019) 1140–1151.
[9] R. Ma, T. Liu, Z. Luo, Q. Guo, Y. Xiao, Y. Chen, X. Li, S. Luo, X. Lu, M. Zhang, Y. Li, H. Yan, Sci. China: Chem. 63 (2020) 325–330.
[10] W. Gao, H. Fu, Y. Li, F. Lin, R. Sun, Z. Wu, X. Wu, C. Zhong, J. Min, J. Luo, H. Y. Woo, Z. Zhu, A.-K.-Y. Jen, Adv. Energy Mater. 11 (2020) 2003177.
[11] D. Li, L. Zhu, X. Liu, W. Xiao, J. Yang, R. Ma, L. Ding, F. Liu, C. Duan, M. Fahlman, Q. Bao, Adv. Mater. 32 (2020) 2002344.
[12] H. Chen, H. Lai, Z. Chen, Y. Zhu, H. Wang, L. Han, Y. Zhang, F. He, Angew. Chem. Int. Ed. 60 (2021) 3238–3246.
[13] X. Guo, Q. Fan, J. Wu, G. Li, Z. Peng, W. Su, J. Lin, L. Hou, Y. Qin, H. Ade, L. Ye, M. Zhang, Y. Li, Angew. Chem. Int. Ed. 60 (2021) 2322–2329.
[14] L. Meng, Y. Zhang, X. Wan, C. Li, X. Zhang, Y. Wang, X. Ke, Z. Xiao, L. Ding, R. Xia, H.-L. Yip, Y. Cao, Y. Chen, Science 361 (2018) 1094–1098.
[15] Z. Zhang, Y. Li, G. Cai, Y. Zhang, X. Lu, Y. Lin, J. Am. Chem. Soc. 142 (2020) 18741–18745.
[16] F. Lin, K. Jiang, W. Kaminsky, Z. Zhu, A.-K.-Y. Jen, J. Am. Chem. Soc. 142 (2020) 15246–15251.
[17] C. Zhu, J. Yuan, F. Cai, L. Meng, H. Zhang, H. Chen, J. Li, B. Qiu, H. Peng, S. Chen, Y. Hu, C. Yang, F. Gao, Y. Zou, Y. Li, Energy Environ. Sci. 13 (2020) 2459–2466.
[18] X. Xu, L. Yu, H. Yan, R. Li, Q. Peng, Energy Environ. Sci. 13 (2020) 4381–4388.
[19] Y.-J. Cheng, S.-H. Yang, C.-S. Hsu, Chem. Rev. 109 (2009) 5868–5923.
[20] H. Zhou, L. Yang, W. You, Macromolecules 45 (2012) 607–632.
[21] Y. Chen, F. Bai, Z. Peng, L. Zhu, J. Zhang, X. Zou, Y. Qin, H.K. Kim, J. Yuan, L.-K. Ma, J. Zhang, H. Yu, P.C.Y. Chow, F. Huang, Y. Zou, H. Ade, F. Liu, H. Yan, Adv. Energy Mater. 11 (2021) 2003141.
[22] X. Shi, L. Zuo, S.B. Jo, K. Gao, F. Lin, F. Liu, A.-K.-Y. Jen, Chem. Mater. 29 (2017) 8369–8376.
[23] J. Zhu, Y. Xiao, J. Wang, K. Liu, H. Jiang, Y. Lin, X. Lu, X. Zhan, Chem. Mater. 30 (2018) 4150–4156.
[24] W. Peng, G. Zhang, M. Zhu, H. Xia, Y. Zhang, H. Tan, Y. Liu, W. Chi, Q. Peng, W. Zhu, A.C.S. Appl, Mater. Interfaces 11 (2019) 48128–48133.
[25] Z. Xiao, F. Liu, X. Geng, J. Zhang, S. Wang, Y. Xie, Z. Li, H. Yang, Y. Yuan, L. Ding, Sci. Bull. 62 (2017) 1331–1336.
[26] Z. Xiao, X. Jia, D. Li, S. Wang, X. Geng, F. Liu, J. Chen, S. Yang, T.P. Russell, L. Ding, Sci. Bull. 62 (2017) 1494–1496.
[27] Z. Xiao, X. Jia, L. Ding, Sci. Bull. 62 (2017) 1562–1564.
[28] Z. Xiao, S. Yang, Z. Yang, J. Yang, H.-L. Yip, F. Zhang, F. He, T. Wang, J. Wang, Y. Yuan, H. Yang, M. Wang, L. Ding, Adv. Mater. 31 (2019) 1804790.
[29] Y. Tong, Z. Xiao, X. Du, C. Zuo, Y. Li, M. Lv, Y. Yuan, C. Yi, F. Hao, Y. Hua, T. Lei, Q. Lin, K. Sun, D. Zhao, C. Duan, X. Shao, W. Li, H.-L. Yip, Z. Xiao, B. Zhang, Q. Bian, Y. Cheng, S. Liu, M. Cheng, Z. Jin, S. Yang, L. Ding, Sci China: Chem. 63 (2020) 758–765.
[30] S. Beaupré, P.-L.-T. Boudreault, M. Leclerc, Adv. Mater. 22 (2010) E6–E27.
[31] Y. Geng, A. Tang, K. Tajima, Q. Zeng, E. Zhou, J. Mater. Chem. A 7 (2019) 64–96.
[32] K.H. Hendriks, W. Li, M.M. Wienk, R.A.J. Janssen, J. Am. Chem. Soc. 136 (2014) 12130–12136.
[33] T.-W. Chen, C.-C. Chang, Y.-T. Hsiao, C. Chan, L. Hong, L. Zhong, W.-T. Chuang, J. Hou, Y. Li, C.-S. Hsu, A.C.S. Appl, Mater. Interfaces 11 (2019) 31069–31077.
[34] T.-W. Chen, Y.-T. Hsiao, Y.-W. Lin, C.-C. Chang, W.-T. Chuang, Y. Li, C.-S. Hsu, Mater. Chem. Front. 3 (2019) 829–835.
[35] S.-L. Chang, K.-E. Hung, F.-Y. Cao, K.-H. Huang, C.-S. Hsu, C.-Y. Liao, C.-H. Lee, Y.-J. Cheng, A.C.S. Appl, Mater. Interfaces 11 (2019) 33179–33187.
[36] Q. Cao, W. Xiong, H. Chen, G. Cai, G. Wang, L. Zheng, Y. Sun, J. Mater. Chem. A 5 (2017) 7451–7461.
[37] Q. Tu, Y. Ma, X. Zhou, W. Ma, Q. Zheng, Chem. Mater. 31 (2019) 5953–5963.
[38] H. Wang, Z. Zhang, J. Yu, X. Liu, S. Qu, S. Guang, W. Tang, J. Mater. Chem. A 7 (2019) 21903–21910.
[39] J. Ouyang, G. Zeng, Y. Xin, X. Zhao, X. Yang, Sol. RRL 4 (2019) 1900417.
[40] J. Sun, X. Ma, Z. Zhang, J. Yu, J. Zhou, X. Yin, L. Yang, R. Geng, R. Zhu, F. Zhang, W. Tang, Adv. Mater. 30 (2018) 1707150.
[41] J. Cao, H. Wang, S. Qu, J. Yu, L. Yang, Z. Zhang, F. Du, W. Tang, Adv. Funct. Mater. 30 (2020) 2006141.
[42] H. Huang, M. Qiu, Q. Li, S. Liu, X. Zhang, Z. Wang, N. Fu, B. Zhao, R. Yang, W. Huang, J. Mater. Chem. C 4 (2016) 5448–5460.
[43] Y.K. Eom, S.H. Kang, I.T. Choi, Y. Yoo, J. Kim, H.K. Kim, J. Mater. Chem. A 5 (2017) 2297–2308.
[44] L. Liu, Y. Wu, M. Li, X. Zong, Z. Sun, M. Liang, S. Xue, Chem. Commun. 54 (2018) 14025–14028.
[45] J. Yang, Y. Cai, Y. Zhou, C. Zhang, P. Liang, B. Zhao, J. Shao, N. Fu, W. Huang, X. Dong, Dyes Pigments 147 (2017) 270–282.
[46] L. Zhan, S. Li, T.-K. Lau, Y. Cui, X. Lu, M. Shi, C.-Z. Li, H. Li, J. Hou, H. Chen, Energy Environ. Sci. 13 (2020) 635–645.
[47] H. Wang, Z. Zhang, X. Liu, S. Qu, S. Guang, Z. Ye, J. Yu, W. Tang, Chem. Eng. J. 413 (2021), 127444.
[48] J. Gao, X. Ma, C. Xu, X. Wang, J.H. Son, S.Y. Jeong, Y. Zhang, C. Zhang, K. Wang, L. Niu, J. Zhang, H.Y. Woo, J. Zhang, F. Zhang, Chem. Eng. J. 413 (2021), 129276.
[49] K. Jin, Z. Xiao, L. Ding, J. Semicond. 42 (2021), 060502.
[50] W. Zhao, S. Li, H. Yao, S. Zhang, Y. Zhang, B. Yang, J. Hou, J. Am. Chem. Soc. 139 (2017) 7148–7151.
[51] Y. Qin, Y. Xu, Z. Peng, J. Hou, H. Ade, Adv. Funct. Mater. 30 (2020) 2005011.
[52] W. Peng, G. Zhang, L. Shao, C. Ma, B. Zhang, W. Chi, Q. Peng, W. Zhu, J. Mater. Chem. A 6 (2018) 24267–24276.
[53] B. Qiu, J. Yuan, Y. Zou, D. He, H. Peng, Y. Li, Z. Zhang, Org. Electron. 35 (2016) 87–94.
[54] J. Pommerehne, H. Vestweber, W. Guss, R.F. Mahrt, H. Bässler, M. Porsch, J. Daub, Adv. Mater. 7 (1995) 551–554.
[55] H. Tan, X. Zheng, J. Zhu, J. Yu, W. Zhu, J. Mater. Chem. C 7 (2019) 13301–13306.
[56] Z. Zhang, L. Feng, S. Xu, Y. Liu, H. Peng, Z.-G. Zhang, Y. Li, Y. Zou, Adv. Sci. 4 (2017) 1700152.
[57] S. Liu, W. Su, X. Zou, X. Du, J. Cao, N. Wang, X. Shen, X. Geng, Z. Tang, A. Yartsev, M. Zhang, W. Gruber, T. Unruh, N. Li, D. Yu, C.J. Brabece, E. Wang, J. Mater. Chem. A 8 (2020) 5995–6003.
[58] R. Wang, C. Zhang, Q. Li, Z. Zhang, X. Wang, M. Xiao, J. Am. Chem. Soc. 142 (2020) 12751–12759.
[59] T. Lu, F. Chen, J. Comput. Chem. 33 (2012) 580–592.
[60] S. Du, N. Yao, S. Liu, Y. Xu, J. Cao, W. Zhuang, J. Yu, N. Wang, D. Yu, F. Zhang, E. Wang, Dyes Pigments 185 (2021), 108892.
[61] R. Cammi, B. Mennucci, J. Chem. Phys. 110 (1999) 9877–9886.
[62] R. Improta, V. Barone, G. Scalmani, M.J. Frisch, J. Chem. Phys. 125 (2006), 054103.
[63] G. Xie, Z. Zhang, Z. Su, X. Zhang, J. Zhang, Nano Energy 69 (2020), 104447.
[64] B. Qiu, S. Chen, H. Li, Z. Luo, J. Yao, C. Sun, X. Li, L. Xue, Z.-G. Zhang, C. Yang, Y. Li, Chem. Mater. 31 (2019) 6558–6567.
[65] P.W.M. Blom, V.D. Mihailetchi, L.J.A. Koster, D.E. Markov, Adv. Mater. 19 (2007) 1551–1566.
[66] C. Li, H. Fu, T. Xia, Y. Sun, Adv. Energy Mater. 9 (2019) 1900999.
[67] L. Zhang, X. Xu, B. Lin, H. Zhao, T. Li, J. Xin, Z. Bi, G. Qiu, S. Guo, K. Zhou, X. Zhan, W. Ma, Adv. Mater. 30 (2018) 1805041.

[68] R. Wang, J. Yuan, R. Wang, G. Han, T. Huang, W. Huang, J. Xue, H.-C. Wang, C. Zhang, C. Zhu, P. Cheng, D. Meng, Y. Yi, K.-H. Wei, Y. Zou, Y. Yang, Adv. Mater. 31 (2019) 1904215.
[69] R. Ma, T. Liu, Z. Luo, K. Gao, K. Chen, G. Zhang, W. Gao, Y. Xiao, T.-K. Lau, Q. Fan, Y. Chen, L.-K. Ma, H. Sun, G. Cai, T. Yang, X. Lu, E. Wang, C. Yang, A.-K.-Y. Jen, H. Yan, ACS Energy Lett. 5 (2020) 2711–2720.
[70] L. Qin, X. Liu, X. Zhang, J. Yu, L. Yang, F. Zhao, M. Huang, K. Wang, X. Wu, Y. Li, H. Chen, K. Wang, J. Xia, X. Lu, F. Gao, Y. Yi, H. Huang, Angew. Chem. Int. Ed. 59 (2020) 15043–15049.